



Communication

Quantum linear magnetoresistance in NbTe₂Hongxiang Chen^{a,b}, Zhilin Li^a, Xiao Fan^{a,b}, Liwei Guo^{a,**}, Xiaolong Chen^{a,c,d,*}^a Research & Development Center for Functional Crystals, Beijing National Laboratory for Condensed Matter Physics, Institute of Physics, Chinese Academy of Sciences, Beijing 100190, China^b University of Chinese Academy of Sciences, Beijing 100049, China^c School of Physical Sciences, University of Chinese Academy of Sciences, Beijing 101408, China^d Collaborative Innovation Center of Quantum Matter, Beijing 100084, China

ARTICLE INFO

Communicated by D.D. Sarma

Keywords:

- A. NbTe₂
- B. Linear magnetoresistance
- C. Charge density wave
- D. Anisotropy

ABSTRACT

NbTe₂ is a quasi-2D layered semimetal with charge density wave ground state showing a distorted-1T structure at room temperature. Here we report the anisotropic magneto-transport properties of NbTe₂. An anomalous linear magnetoresistance up to 30% at 3 K in 9 T was observed, which can be well explained by a quantum linear magnetoresistance model. Our results reveal that a large quasi-2D Fermi surface and small Fermi pockets with linearly dispersive bands coexist in NbTe₂. The comparison with the isostructural TaTe₂ provides more information about the band structure evolution with charge density wave transitions in NbTe₂ and TaTe₂.

1. Introduction

Transition metal dichalcogenides (TMDCs), MX₂ (M = transition metal, X = S, Se, or Te), are a series of layered compounds with weak interlayer interactions governed by van der Waals forces. Depending on constituent elements M and X, these dichalcogenides can vary from semiconducting to metallic and even superconducting in transport property [1]. The diversity in properties and their sensitivity to thickness [2,3] have drawn much attention recently. Since Te atom is less negative than S and Se atoms in electronegativity, so more charge is expected to transfer [4] from p bands of Te to the d bands of metal M, leading to an oxidation state M^{(4-ε)⁺} in MTe₂. The charge-transfer results in structural distortions and then unusual properties ensue. Recently, considerable attention has been paid on the intrinsic properties of MTe₂ and many fascinating phenomena like new Fermions [5], extreme large magnetoresistance(MR) [6], linear MR [7], and superconductivity [8,9] were found in WTe₂, TaTe₂, doped or intercalated IrTe₂ and etc.

We have previously studied the magneto-transport and magnetic properties of the low temperature phase of TaTe₂ (LT-TaTe₂) [7]. Shortly after our report, the superconductivity with T_c ~ 4 K under high pressures in TaTe₂ was found [10]. TaTe₂ and NbTe₂ are isostructural and both show double-zigzag chain-like metal atom modulations at room temperature [11]. The double-zigzag chain-like structure was observed in the

surface morphology studied by transmission electron microscope (TEM) [12,13], scanning tunneling microscope (STM) [14], and low energy electron diffraction (LEED) [14,15]. Besides, an intriguing metastable phase under heat pulses [16] or electron beam irradiations of a certain dose [15] has been detected. Similar to NbSe₂ [17] and doped or intercalated IrTe₂, NbTe₂ shows a coexistence of charge density wave (CDW) and superconductivity [18,19]. The superconductivity was found below 0.74 K in NbTe₂. Interestingly, it was found the low critical field H_{c1} is extremely small, less than 0.5 Oe. Unlike TaTe₂, NbTe₂ does not show a further clustering at low temperatures as appeared in LT-TaTe₂. Instead, it exists a structure transition from distorted-1T(1T') phase to 1T phase when temperature is above 550 K (as shown in Fig. 1(a)) [20]. Hence, NbTe₂ is a better platform to study the structural and electronic properties of 1T' phase.

The energy band structure and Fermi surface of 1T'-NbTe₂ have been studied by first-principle calculations and angle-resolved photoelectron emission spectroscopy (ARPES) [14]. The detected Fermi surface is diffusive and an experimental study on the magneto-transport properties in NbTe₂ is still lacking. Here, we present a systematical study on the anisotropic magneto-transport properties of 1T'-NbTe₂. A detailed comparison in anisotropic magneto-transport properties between NbTe₂ and TaTe₂ is given to clarify the origin of the quantum linear MR in both materials. Our results on magneto-transport properties of NbTe₂ are

* Corresponding author. Research & Development Center for Functional Crystals, Beijing National Laboratory for Condensed Matter Physics, Institute of Physics, Chinese Academy of Sciences, Beijing 100190, China.

** Corresponding author.

E-mail addresses: lwguo@iphy.ac.cn (L. Guo), chenx29@iphy.ac.cn (X. Chen).

<https://doi.org/10.1016/j.ssc.2018.02.019>

Received 19 September 2017; Received in revised form 23 February 2018; Accepted 28 February 2018

Available online 7 March 2018

0038-1098/© 2018 Elsevier Ltd. All rights reserved.

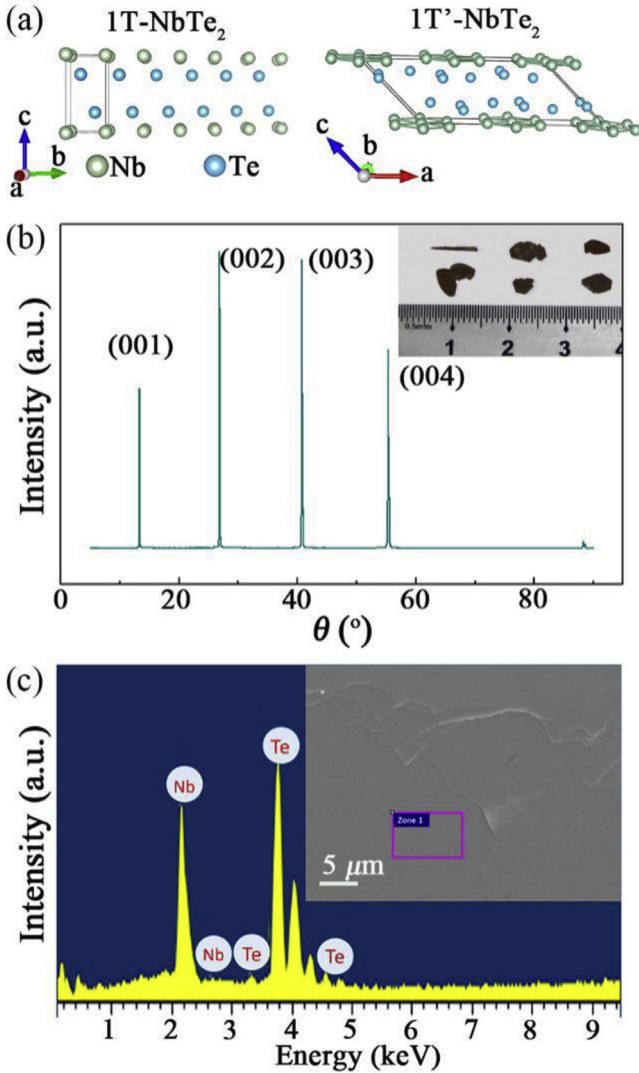


Fig. 1. (a) Schematic crystal structures of 1T-NbTe₂ and 1T'-NbTe₂. The solid lines indicate the unit cells. (b) X-ray diffraction pattern of a TaTe₂ single crystal measured at room temperature. Inset: an optical image of typical single crystals from different batches. (c) The energy spectrum data of a cleaved sample surface. Inset: SEM morphology of a cleaved NbTe₂ sample surface. The square indicates the analyzed zone of EDX analysis on a sample surface.

helpful to reveal the electronic structure evolution with CDW transitions in NbTe₂ and TaTe₂.

2. Material and methods

Single crystals of NbTe₂ were grown by an improved chemical vapor transport (CVT) method [21,22]. Niobium foil (99.99%), Te powder (99.99%), and little amount of iodine (99%) were loaded into an evacuated silica tube in cross section diameter of 1 cm and long 15 cm. The tube was heated in a two-zone furnace at 550 °C for 1 day, and then rise the temperature to 850 °C at the hot end and 750 °C at the cool end. Maintaining this temperature gradient for one week and then cooled naturally, crystals with metal luster were obtained (See the inset of Fig. 1(b) at the cool end. The crystals are usually thin platelets oriented along [001] or long ribbons, and over half centimeters in at least one dimension. The composition of the prepared NbTe₂ sample was checked by energy-dispersive x-ray analysis (EDX). X-ray diffraction (XRD) pattern was collected using a PANalytical X'Pert PRO diffractometer with Cu radiation.

The resistivity measurements were performed on a Quantum Design

physical property measurement system (PPMS) with highest magnetic field of 9 T. A standard four probes technique is applied to measure the in-plane resistivity and the MR defined as $(\rho_{xx}(B, T) - \rho_{xx}(0, T))/\rho_{xx}(0, T)$. Field and temperature dependent Hall resistance $R_{xy}(B, T)$ measurements were carried out using a six-probes method. Angle-dependent MRs (ADMR) were measured using a rotation option of PPMS.

3. Results and discussion

3.1. XRD and EDX analysis of NbTe₂

The single crystal samples were checked by XRD (Fig. 1(b)). The strong diffraction peaks can be indexed as (00l), consistent with the ICDD-PDF 21-0605. Fig. 1(a) presents the crystal structure of 1T'-NbTe₂ (Space group C2/m (No. 12), Z = 6, a = 19.39 Å, b = 3.642 Å, c = 9.375 Å, $\beta = 134.58^\circ$) [11]. The single crystals are brittle and can be easily cleaved along (001) plane. The layered characteristics can be found in the SEM image showing thin platelets. The cleaved plane is flat and clean without any iodine trace left as supported by EDX data of Fig. 1(c). The EDX indicated the composition of Nb:Te = 35:65, in well agreement with the ratio of chemical stoichiometry of NbTe₂. According to the experimental data of XRD and the EDX analysis, we confirmed the crystals are NbTe₂.

3.2. Magneto-transport properties of 1T'-NbTe₂

We measured the temperature-dependent resistivity of several samples from different batches and found the residual resistance ratio ($RRR = \rho_{xx}(300 \text{ K})/\rho_{xx}(3 \text{ K})$) values are in the range of 10–20. We chose the sample with $RRR \sim 20$ to study its magneto-transport properties in detail. The resistivity of NbTe₂ is 115.5 $\mu\Omega \text{ cm}$ at 300 K, and 5.8 $\mu\Omega \text{ cm}$ at 3 K. The in-plane resistivity $\rho_{xx}(0, T)$ (Fig. 2(a)) shows a typical metallic behaviour. A small thermal hysteresis is observed near room temperature between the cooling and warming cycles with a rate of 5 K/min. Hall resistances at different temperatures are shown in Fig. 2(b). All the Hall resistances show a positive linear dependence on magnetic field B , which indicates that almost no carrier concentration changed with increasing field and the dominant charge carriers in NbTe₂ are holes, similar to that in TaTe₂. The Hall coefficient, $R_H = d\rho_{xy}(B)/dB$, increases with increasing temperature, which is opposite to LT-TaTe₂. The net carrier concentration is given by $(n_h - n_e) = 1/(eR_H)$ and the carrier mobility is given by $\mu = R_H/\rho_{xx}$. The carrier concentration $(n_h - n_e)$ and mobility both decrease with increasing temperature as shown in Fig. 2(c). The net carrier concentration $(n_h - n_e)$ is about $1.7 \times 10^{21} \text{ cm}^{-3}$ and the mobility is about 607 $\text{cm}^2/(\text{V s})$ at 3 K.

The transverse MRs versus magnetic field at low temperatures are presented in Fig. 3(a). A relatively large MR reached 30% was observed under a 9 T field at 3 K and did not show any signs of saturation in measured field range. A crossover of MRs from a semi-classical weak-field B^2 dependence to a nearly linear B dependence was observed when the magnetic field is beyond a critical field B^* . In order to determine the critical field B^* , the differential MR versus field, dMR/dB , is plotted as shown in Fig. 3(b) dMR/dB is linearly proportional to B with a large positive slope in low fields, but reached a much reduced slope when field is higher than B^* ($B^* \sim 1.85 \text{ T}$ at 3 K), which is determined by an intersection of two linear fitting lines (as shown by the guide lines in Fig. 3(b)). The critical field shifts to a higher field with increasing temperature, as shown in Fig. 3(c). The dependence of the critical field B^* on temperature is shown with blue square in Fig. 3(d), which can be well fitted with the red solid curve satisfying $B^* = (1/2e\hbar v_F^2)(EF + kBT)^2$ with $v_F \approx 5.7(3) \times 10^4 \text{ m/s}$ and $E_F \approx 8.2(3) \text{ meV}$. The critical field dependence on temperature suggested the existence of electronic band with linear dispersion [23] in 1T'-NbTe₂ and will be discussed in the following.

From the Hall resistance measurements, the carrier concentration of NbTe₂ can be deduced to be in the order of $10^{20} \sim 10^{21} \text{ cm}^{-3}$, which is

much higher than the quantum limit to observe a quantum linear MR [24], but similar to the case in LT-TaTe₂ [7]. Therefore, here we discuss the linear MR of NbTe₂ with the model of quantum linear MR in layered semimetals proposed by Abrikosov [25]. The high carrier concentration in quasi-2D materials indicates the existence of relatively large normal Fermi surface in 1T'-NbTe₂. According to the quantum model of Abrikosov [25], the linear MR in 1T'-NbTe₂ suggests that apart from the large Fermi surface exists in 1T'-NbTe₂, there should exist some small Fermi pockets with almost linear band dispersions in NbTe₂. As well known, an

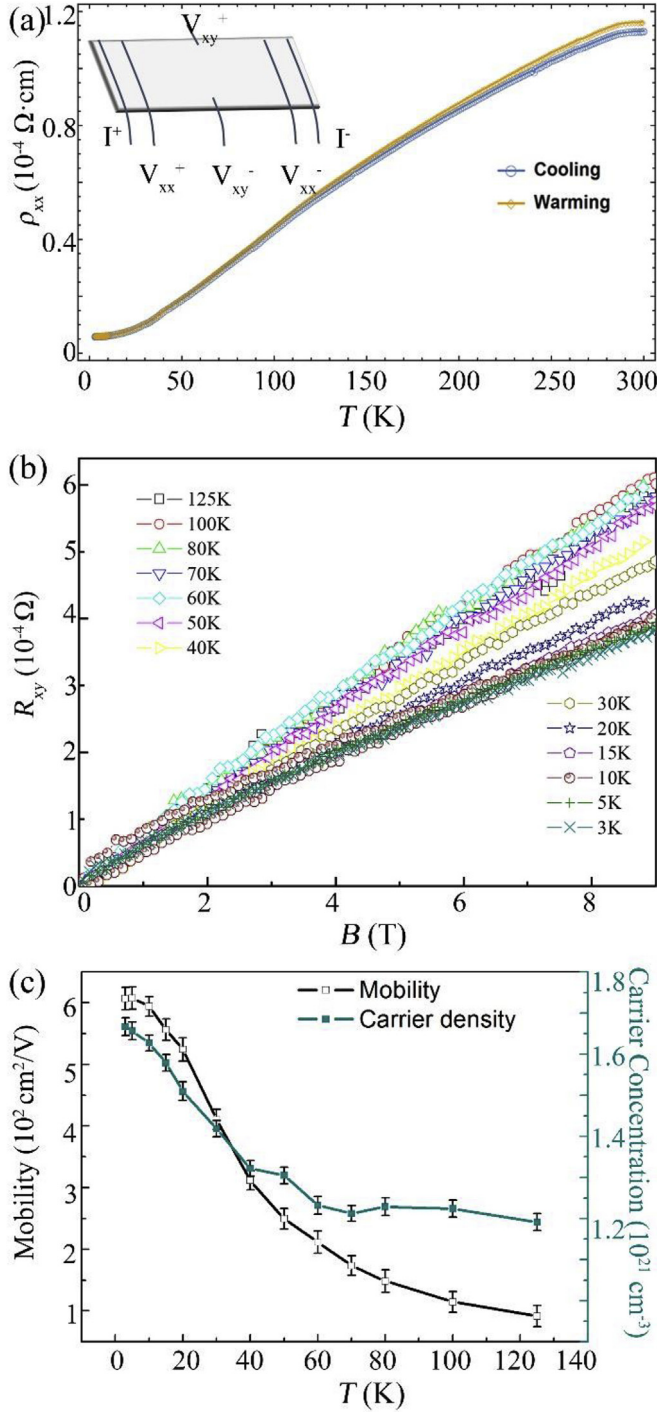


Fig. 2. (a) Temperature dependent resistivity of 1T'-NbTe₂. Inset: the configuration of six-probes method. (b) The field dependence of Hall resistance (R_{xy}) at different temperatures. (c) Temperature dependence of carrier concentration and mobility.

applied magnetic field will induce the Landau level (LL) splitting. In the quantum limit at a specific temperature and a field, LL spacing becomes larger than both the Fermi energy E_F and the thermal fluctuations $k_B T$. Consequently, only the lowest Landau level is occupied for the small Fermi pockets and a quantum linear MR ensues [24].

For energy band with linear dispersion [26], the splitting between the lowest and the first Landau level can be described by $\Delta_1 = |E_{\pm 1} - E_0| = \pm v_F \sqrt{2\hbar e B}$, where v_F is the Fermi velocity. When the quantum limit is approached in a linear energy band, the critical field B^* should satisfy the equation $B^* = (1/2ehv_F^2)(E_F + k_B T)^2$ [23]. As shown in Fig. 3(c), the critical field deduced from our 1T'-NbTe₂ sample could be well fitted by the equation $B^* = (1/2ehv_F^2)(E_F + k_B T)^2$ [23]. The fitting results (See Fig. 3(d)) yield the Fermi level $E_F \approx 8.2(3)$ meV, and the Fermi velocity $v_F \approx 5.7(3) \times 10^4$ m/s. They are about two times larger and 65.2% higher than the values in LT-TaTe₂, respectively. Furthermore, it is deduced that the $\Delta_1 = E_F + k_B T$ at the critical field B^* , satisfying the regime of quantum limit. These results strongly support that the linear MR behaviour originates from the Dirac states formed by the Fermi surface reconstruction in 1T'-NbTe₂.

The MR of NbTe₂ under low temperature and high magnetic field is contributed by both normal carriers and carriers with linear band dispersion. The observed MR is mainly contributed by normal carriers when $B < B^*$, so dMR/dB is linearly proportional to B with a large positive slope. When $B > B^*$, the quantum linear MR contributed by carriers with linear band dispersion will be dominated, whose effect will result in a saturation of dMR/dB at high fields. However, in the case, the MR contributed from normal carriers is still remained, whose effect will lead to a weak dependence on field B . Consequently, as a total effect, dMR/dB will not be saturate to a constant, but show a much weak dependence on field B as shown in Fig. 3(B).

As suggested by the magneto-transport behaviors of NbTe₂, the Fermi surface of NbTe₂ are composed by the relatively large Fermi pockets and small Fermi pockets with linear band dispersion. While, we observed almost a single band behaviour in the Hall resistance measurement as shown in Fig. 2(B). We consider this is due to the carriers transport in NbTe₂ are dominated by holes contributed from the large Fermi surfaces, and the mobility of carriers contributed from different bands may be very close. Meanwhile, according to the quantum linear MR model [25], the carrier density in small Fermi pocket with linear band dispersions is about 10^{18} cm^{-3} . It is three orders of magnitude lower than that in the normal states, $\sim 10^{21} \text{ cm}^{-3}$, and hence can be neglected in Hall resistance contribution compared with that of the normal carriers. Besides, in our work, the highest measured magnetic field is 9 T, and we think the multi-band feature may be observed under higher fields.

3.3. ADMR of 1T'-NbTe₂

The ADMR at azimuth angle $\varphi = 90^\circ$ are shown in Fig. 4(a) and (b). When $\varphi = 90^\circ$, the magnetic field is perpendicular to the flowing current along the b axis. The detailed geometry of ADMR measurements, polar angle θ and azimuth angle φ are defined in the inset of Fig. 4(a), where a field dependent MR at several angles of $\theta = 0^\circ, 30^\circ, 60^\circ$, and 90° are measured. It is noted a linear MR is observed at each polar angle at high fields. Furthermore, the ADMR at 5 K in 9 T is shown in Fig. 4(b). It is seen that the ADMR has maximums (MR = 30%) when $\theta = 0^\circ$ and 180° . The MR decreases to minimums (MR = 17%) at $\theta = 90^\circ$ and 270° , which decreases by about 43% compared to the maximum. The ADMR could be well fitted by a function of $|\cos\theta|$ as shown in Fig. 4(b), which indicates a quasi-2D Fermi surface [27] exists in 1T'-NbTe₂. But the slight deviation implies existence of three dimensional electronic transport in 1T'-NbTe₂ as reported in the similar material [28].

4. Discussion

Linear MR under high field seems widely exist in layered CDW and

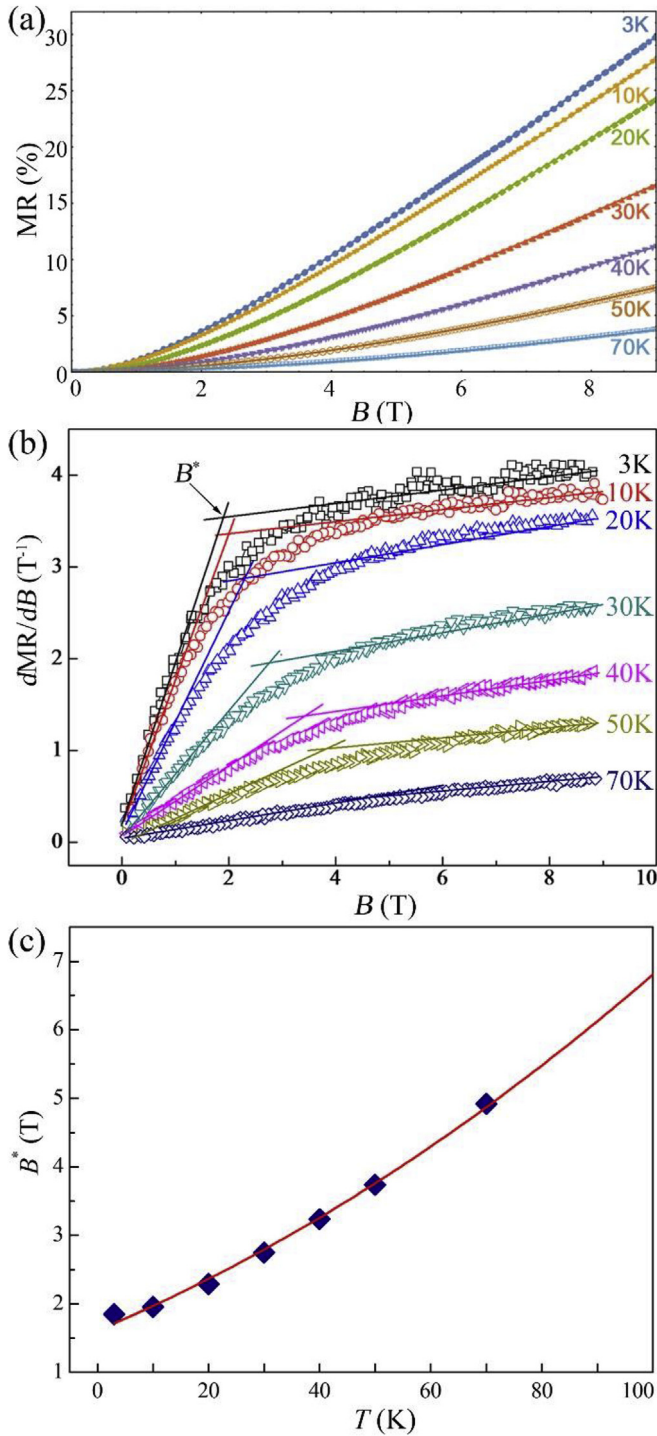


Fig. 3. (a) Magnetic field dependent MR at different temperatures. (b) Dependence of differential MR on magnetic field at different temperatures. A critical field B^* is defined as the intersection between the two fitting lines for dMR/dB against B in low field semi-classical regime and high field quantum regime. (c) Dependence of critical field B^* on temperature, data are marked by blue squares.

spin density wave (SDW) compounds, such as iron pnictides [23,29], 2H-NbSe₂, 2H-TaSe₂ [30], LT-TaTe₂ and so on. The MRs in these materials are relatively large but smaller than that in some Dirac or Weyl semimetals [31–34] and compensated semimetals [6,35]. The linear MR in 1T'-NbTe₂ is quite similar to that of LT-TaTe₂. At room temperature, NbTe₂ and TaTe₂ both are 1T' structure, while TaTe₂ shows a further clustering along b axis below 170 K, which is absent in NbTe₂. While 1T'-NbTe₂ transforms into the 1T phase when temperature is higher than

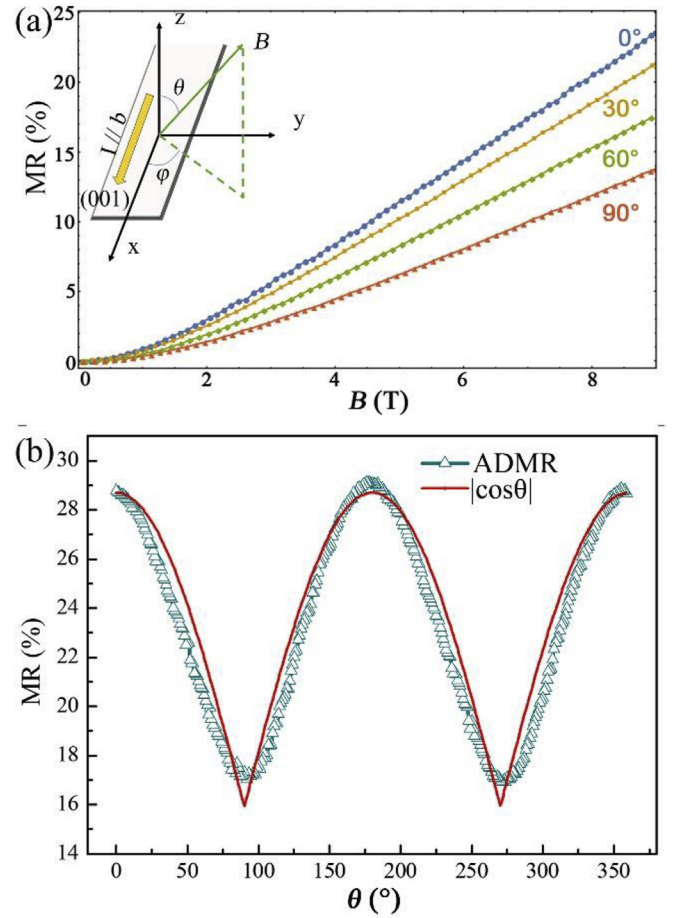


Fig. 4. Anisotropic MRs (a) Polar angle θ ($\varphi = 90^\circ$) dependent MR at 5 K in 9 T. The fitting curve fitted by the function of $|\cos\theta|$ is shown by the red curve. (b) Field dependent MR at four θ angles ($\theta = 0^\circ, 30^\circ, 60^\circ$, and 90°). Inset: the geometry of angle dependent MR measurements.

550 K. As we all know, the CDW transition is accompanied by complicated band-folding [36], and may induced a band with linear dispersion. Linear MRs are observed in both of 1T'-NbTe₂ and LT-TaTe₂, and can be well explained by the quantum linear MR model. So we suggest that the linear MR in 1T'-NbTe₂ and LT-TaTe₂ should be resulted from the Fermi pockets with linearly dispersive bands in the 1T' phase. In our previous LT-TaTe₂ results, MR shows complicated anisotropy with a two-fold symmetry at low temperatures and high fields which revealed the anisotropy of the small Fermi pockets in Dirac states, while here a simple two-fold symmetric anisotropy was found in 1T'-NbTe₂ indicating there exists relatively simple small Fermi pockets with linearly dispersive bands.

5. Conclusions

In conclusion, anisotropic magneto-transport properties of 1T'-NbTe₂ were studied systematically based on high quality single crystals of NbTe₂ with RRR = 20. Carrier concentration and mobility of NbTe₂ both decreases with increasing temperature. The high carrier concentration around 10^{21} cm^{-3} indicates the existence of relatively large normal Fermi surface. The observed anisotropic linear MR at low temperatures under high fields suggests existing a quasi-2D characteristic in Fermi surface of 1T'-NbTe₂. The linear MR and the well fitted critical field B^* versus temperature strongly support the inference of existing small Fermi pockets with linearly dispersive bands in 1T'-NbTe₂. The simple two-fold symmetric MR in 1T'-NbTe₂ indicates the small Fermi pockets in 1T'-NbTe₂ possessing relative high symmetry compared with that in LT-

TaTe₂. Our results provide more information about the electronic structure evolutions among 1T, 1T', and LT-TaTe₂ phases.

Acknowledgements

The authors thank Mr. J. Zhang of Institute of Physics, Chinese Academy of Sciences, for helpful discussion. This work is financially supported by the National Natural Science Foundation of China (Grant Nos. 91422303, 51532010, and 5147226).

References

- [1] Q.H. Wang, K. Kalantar-Zadeh, A. Kis, J.N. Coleman, M.S. Strano, *Nat. Nano* 7 (2012) 699–712.
- [2] K.F. Mak, C. Lee, J. Hone, J. Shan, T.F. Heinz, *Phys. Rev. Lett.* 105 (2010) 136805.
- [3] A. Splendiani, L. Sun, Y. Zhang, T. Li, J. Kim, C.-Y. Chim, G. Galli, F. Wang, *Nano Lett.* 10 (2010) 1271–1275.
- [4] E. Canadell, S.P. Jobic, R. Brec, J. Rouxel, M.-H. Whangbo, *J. Solid State Chem.* 99 (1992) 189–199.
- [5] A.A. Soluyanov, D. Gresch, Z. Wang, Q. Wu, M. Troyer, X. Dai, B.A. Bernevig, *Nature* 527 (2015) 495–498.
- [6] M.N. Ali, J. Xiong, S. Flynn, J. Tao, Q.D. Gibson, L.M. Schoop, T. Liang, N. Haldolaarachchige, M. Hirschberger, N.P. Ong, R.J. Cava, *Nature* 514 (2014) 205–208.
- [7] H. Chen, Z. Li, L. Guo, X. Chen, *Europhys. Lett.* 117 (2017), 27009.
- [8] S. Pyon, K. Kudo, M. Nohara, *J. Phys. Soc. Jpn.* 81 (2012), 053701.
- [9] J.J. Yang, Y.J. Choi, Y.S. Oh, A. Hogan, Y. Horibe, K. Kim, B.I. Min, S.W. Cheong, *Phys. Rev. Lett.* 108 (2012), 116402.
- [10] J. Guo, H. Luo, H. Yang, L. Wei, H. Wang, W. Yi, Y. Zhou, Z. Wang, S. Cai, S. Zhang, X. Li, Y. Li, J. Liu, K. Yang, A. Li, J. Li, Q. Wu, R.J. Cava, L. Sun, *arXiv* (1704) 08106.
- [11] B. Brown, *Acta Crystallogr.* 20 (1966) 264–267.
- [12] J. van Landuyt, G. Remaut, S. Amelinckx, *Phys. Status Solidi (B)* 41 (1970) 271–289.
- [13] J. van Landuyt, G. van Tendeloo, S. Amelinckx, *Phys. Status Solidi (A)* 26 (1974) 585–592.
- [14] C. Battaglia, H. Cercellier, F. Clerc, L. Despont, M.G. Garnier, C. Koitzsch, P. Aebi, H. Berger, L. Forró, C. Ambrosch-Draxl, *Phys. Rev. B* 72 (2005), 195114.
- [15] D. Cukjati, A. Prodan, N. Jug, H.J.P. Van Midden, S.W. Hla, H. Böhm, F.W. Boswell, J.C. Bennett, *physica status solidi (a)* 193 (2002) 246–250.
- [16] J. van Landuyt, G. van Tendeloo, S. Amelinckx, *Phys. Status Solidi (A)* 29 (1975) K11–K13.
- [17] E.L. Revolinsky, E.P. Lautenschlager, C.H. Armitage, *Solid State Commun.* 1 (1963) 59–61.
- [18] M.H. Van Maaren, G.M. Schaeffer, *Phys. Lett. A* 24 (1967) 645–646.
- [19] S. Nagata, T. Abe, S. Ebisu, Y. Ishihara, K. Tsutsumi, *J. Phys. Chem. Solid.* 54 (1993) 895–899.
- [20] S. Kari, K. Arne, *Acta Chem. Scand.* 19 (1965) 258–260.
- [21] A. Ubaldini, J. Jacimovic, N. Ubrig, E. Giannini, *Cryst. Growth Des.* 13 (2013) 4453–4459.
- [22] Z. Li, H. Chen, S. Jin, D. Gan, W. Wang, L. Guo, X. Chen, *Cryst. Growth Des.* 16 (2016) 1172–1175.
- [23] K.K. Huynh, Y. Tanabe, K. Tanigaki, *Phys. Rev. Lett.* 106 (2011) 217004.
- [24] A.A. Abrikosov, *Phys. Rev. B* 58 (1998) 2788–2794.
- [25] A.A. Abrikosov, *Phys. Rev. B* 60 (1999) 4231–4234.
- [26] Y.B. Zhang, Y.W. Tan, H.L. Stormer, P. Kim, *Nature* 438 (2005) 201–204.
- [27] A.B. Pippard, *Magnetoresistance in Metals*, Cambridge University Press, Cambridge, UK, 1989.
- [28] K. Wang, D. Graf, H. Lei, S.W. Tozer, C. Petrovic, *Phys. Rev. B* 84 (2011).
- [29] D. Bhoi, P. Mandal, P. Choudhury, S. Pandya, V. Ganesan, *Appl. Phys. Lett.* 98 (2011) 172105.
- [30] M. Naito, S. Tanaka, *J. Phys. Soc. Jpn.* 51 (1982) 228–236.
- [31] T. Liang, Q. Gibson, M.N. Ali, M. Liu, R.J. Cava, N.P. Ong, *Nat. Mater.* 14 (2015) 280–284.
- [32] C. Shekhar, A.K. Nayak, Y. Sun, M. Schmidt, M. Nicklas, I. Leermakers, U. Zeitler, Y. Skourski, J. Wosnitza, Z. Liu, Y. Chen, W. Schnelle, H. Borrmann, Y. Grin, C. Felser, B. Yan, *Nat. Phys.* 11 (2015) 645–649.
- [33] F.F. Tafti, Q.D. Gibson, S.K. Kushwaha, N. Haldolaarachchige, R.J. Cava, *Nat. Phys.* 12 (2016) 272–277.
- [34] Y.-Y. Lv, B.-B. Zhang, X. Li, S.-H. Yao, Y.B. Chen, J. Zhou, S.-T. Zhang, M.-H. Lu, Y.-F. Chen, *Appl. Phys. Lett.* 108 (2016), 244101.
- [35] Z. Yuan, H. Lu, Y. Liu, J. Wang, S. Jia, *Phys. Rev. B* 93 (2016), 184405.
- [36] G. Grüner, *Density Waves in Solids*, Addison-Wesley, Reading, Massachusetts, 1994.